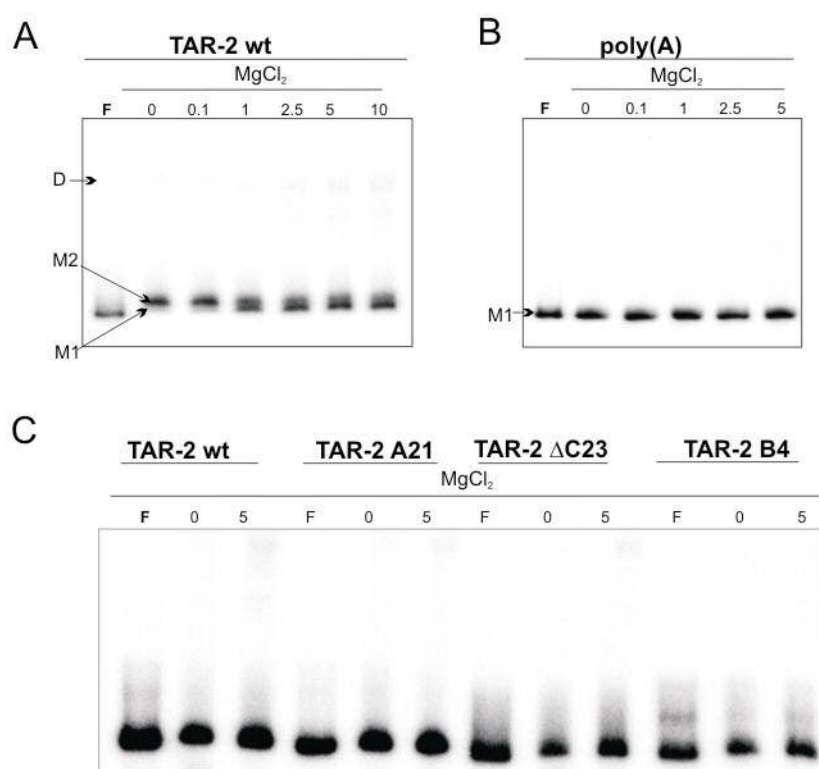


## SUPPLEMENTARY MATERIAL

### New, extended hairpin form of the TAR-2 RNA domain points to the structural polymorphism at the 5' end of the HIV-2 leader RNA

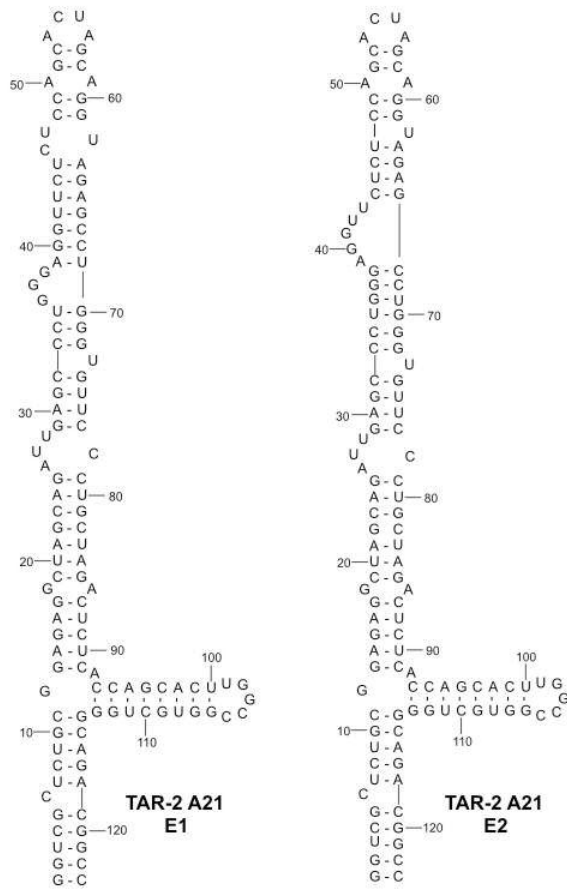
Katarzyna Pachulska-Wieczorek, Katarzyna J. Purzycka and Ryszard W. Adamiak\*

Laboratory of Structural Chemistry of Nucleic Acids, Institute of Bioorganic Chemistry, Polish Academy of Sciences, Noskowskiego 12/14, 61-704 Poznań, Poland

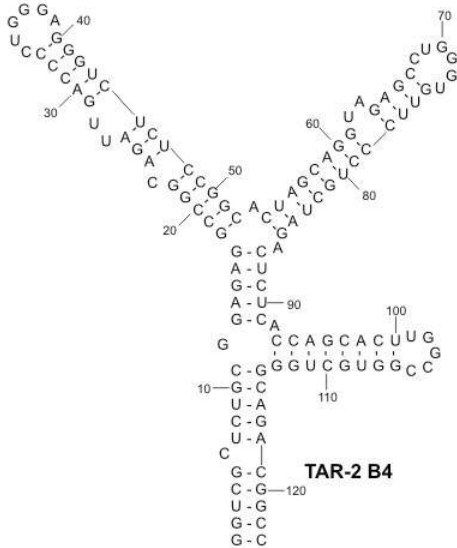


**Figure S1.** Magnesium-dependent mobility of HIV-2 transcripts on non-denaturing PAGE. (A) 123 nt TAR-2 wt, (B) 60 nt poly(A), (C) 123 nt TAR-2 wt and its mutants. Alternatively folded monomeric RNAs are indicated as M and the dimers as D. Lanes F correspond to the formamide-denatured control samples. The samples were analysed on a 6% non-denaturing 0.5×TBE gel (A, C) or 8% non-denaturing 0.5×TB with 0.1% Triton X-100 gel (B). Pattern presented at (C) was obtained at room temperature.

A



B



C

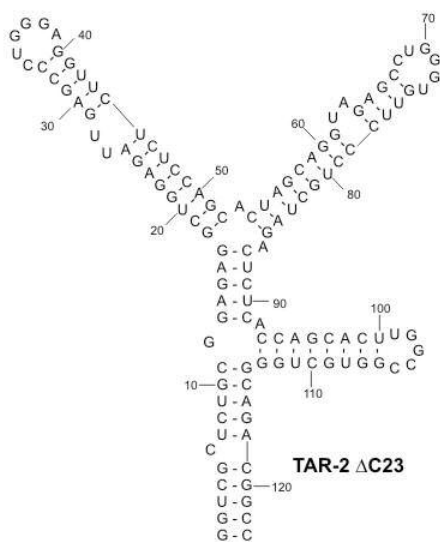


**Figure S2.** Secondary structure models of the TAR-2: (A) A21 mutant represented by two conformers E1 A21 and E2 A21, (B) B4 mutant and (C) ΔC23 mutant (numbering as for TAR-2 wt). The models represent the lowest energy solution given by the Mfold algorithm and are supported by experimental data.



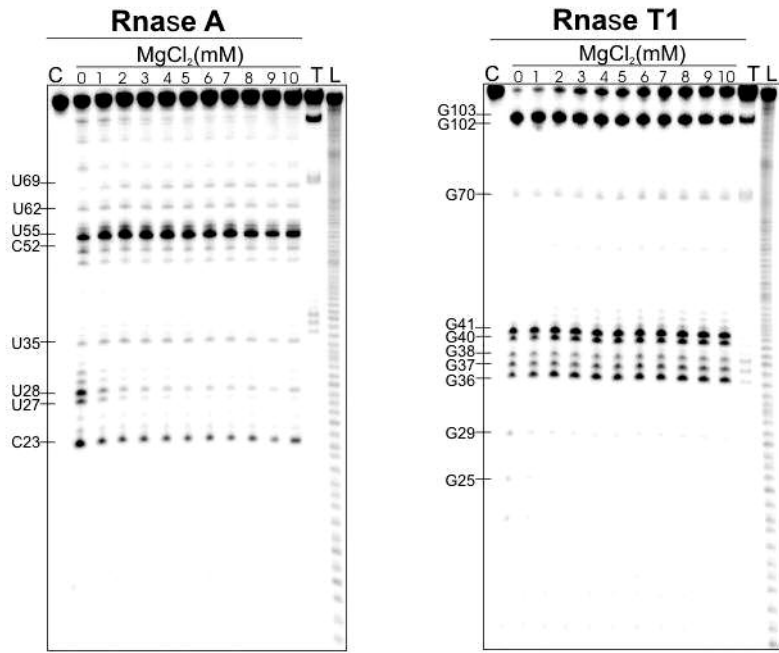


**Figure S4.** Magnesium-dependent secondary structure probing of the TAR-2 wt transcript with RNase A and RNase T1. Lane C represents control samples with untreated RNA; lane L, formamide ladder; lane T, limited hydrolysis with RNase T1. MgCl<sub>2</sub> concentrations (mM) are indicated above the respective lanes.

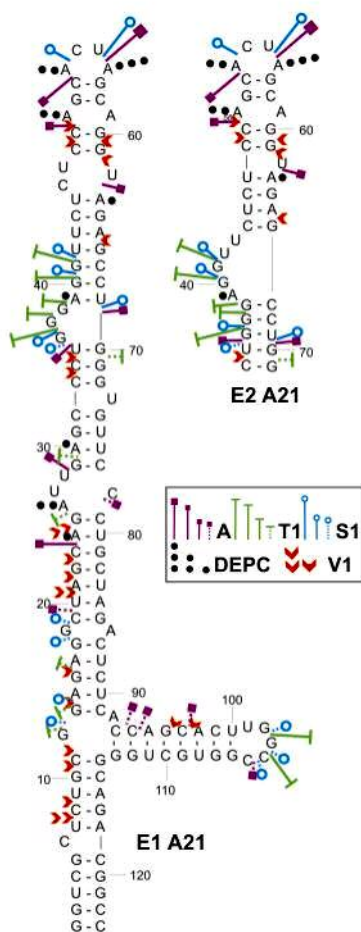


**Figure S5.** A summary of the enzymatic cleavages (S1, T1, A, V1) and chemical modifications (DEPC) data obtained for the 5'-end labelled TAR-2 A21 mutant transcript viewed on the secondary structure models (E1 A21 and E2 A21). For clarity, only the top part of the E2 A21 conformer that differs from E1 A21 is shown. Sites and intensities of cleavages with the respective reagents are indicated by symbols (see insert); size of symbols corresponds to the relative cleavage intensity. The weakest cleavages are not indicated.

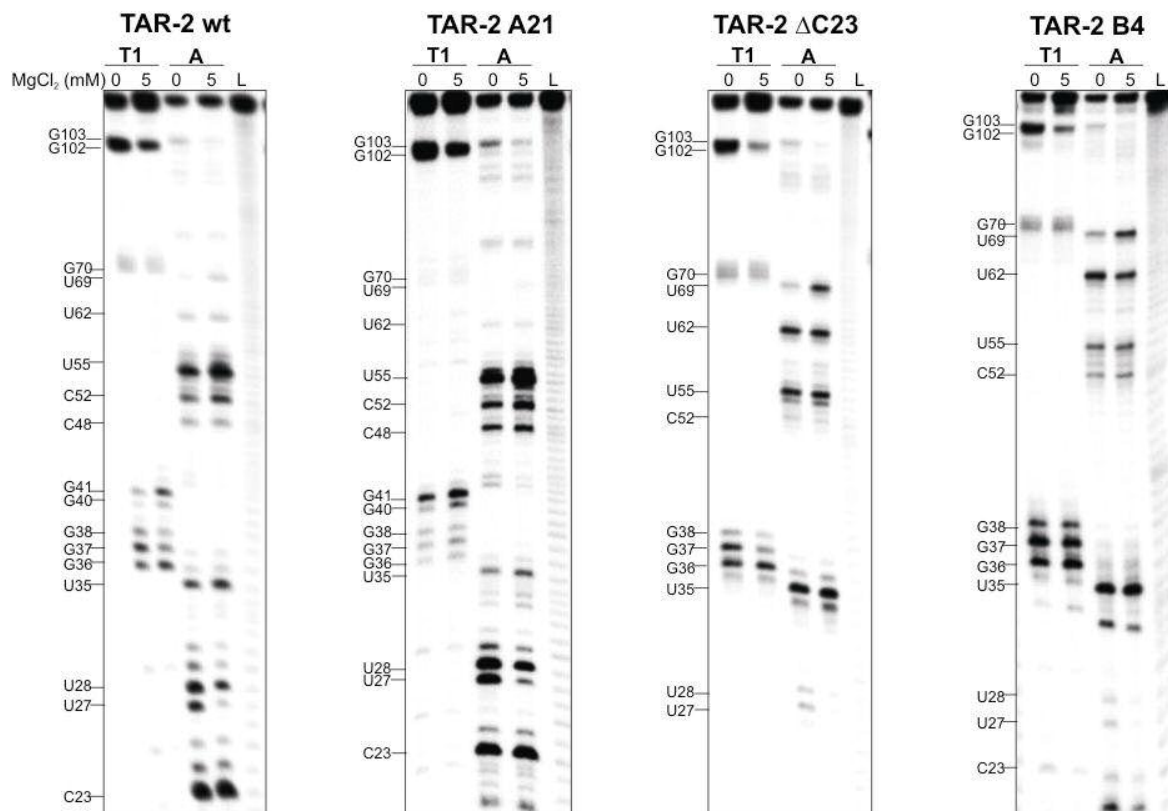


**Figure S6.** RNase T1 and A secondary structure probing of the TAR-2 wt and its mutants stabilized either in extended (A21) or branched ( $\Delta$ C23 and B4) form. MgCl<sub>2</sub> concentrations (mM) are indicated above the respective lanes. Lane L represents the formamide ladder.

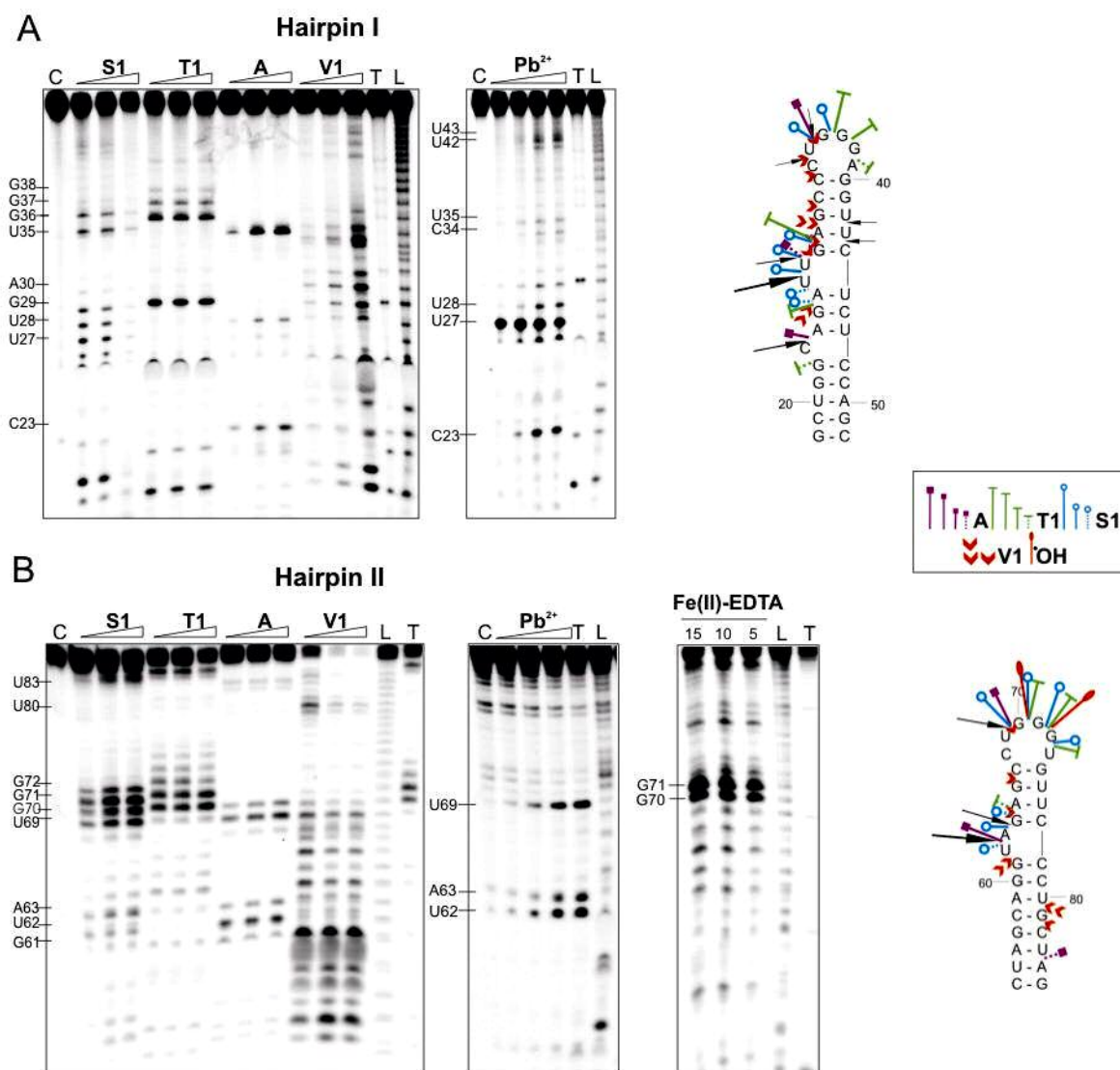


**Figure S7.** Secondary structure probing of the TAR-2 isolated hairpins I (35 nt) and II (32 nt). The RNA was treated with selected single-strand specific enzymes (S1, T1, A), double-strand specific RNase V1, Pb<sup>2+</sup>-ions and with hydroxyl radicals generated by the Fe(II)-EDTA. **(A)** Cleavage patterns obtained for the 5'-end labelled hairpin I. **(B)** Cleavage patterns obtained for the 5'-end labelled hairpin II. Lane C represents control samples with untreated RNA; lane L, formamide ladder; lane T, limited hydrolysis with RNase T1. A summary of the enzymatic and Pb<sup>2+</sup>-induced cleavages or chemical modification (Fe(II)-EDTA) data are viewed on the secondary structure models of the hairpin I **(A)** and II **(B)**. Sites and intensities of cleavages with the respective reagents are indicated by symbols (see insert); size of symbols corresponds to the relative cleavage intensity. The weakest cleavages are not indicated.

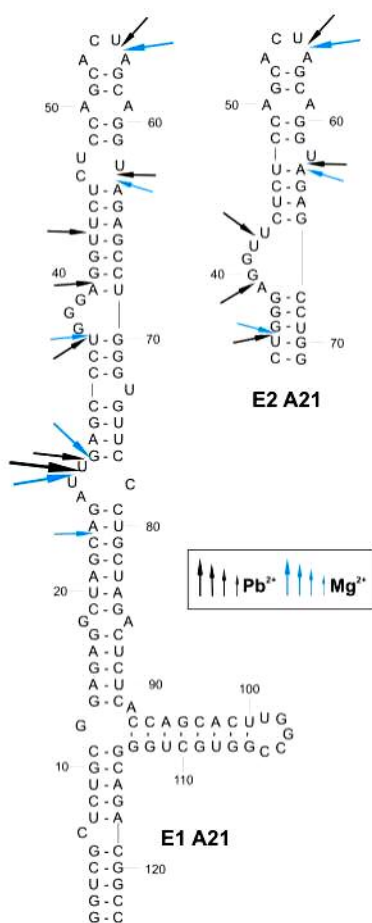


**Figure S8.** A summary of the  $Pb^{2+}$ - and  $Mg^{2+}$ -induced cleavages data obtained for the 5'-end labelled TAR-2 A21 mutant transcript viewed on the secondary structure models (E1 A21 and E2 A21). For clarity, only the top part of the E2 A21 conformer that differs from E1 A21 is shown. Sites and intensities of  $Pb^{2+}$ - and  $Mg^{2+}$ -ions induced cleavages are indicated by arrows (see insert); size of symbols corresponds to the relative intensities. The weakest cleavages are not indicated.

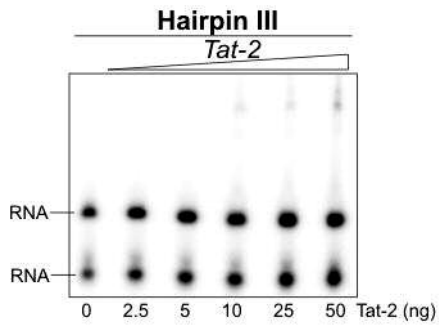


**Figure S9.** Gel shift assay of the Tat-2 binding to the isolated hairpin III present in both TAR-2 forms. RNA hairpin is in equilibrium with duplex. Amounts of the Tat-2 protein (ng per reaction) are indicated below the respective lanes.

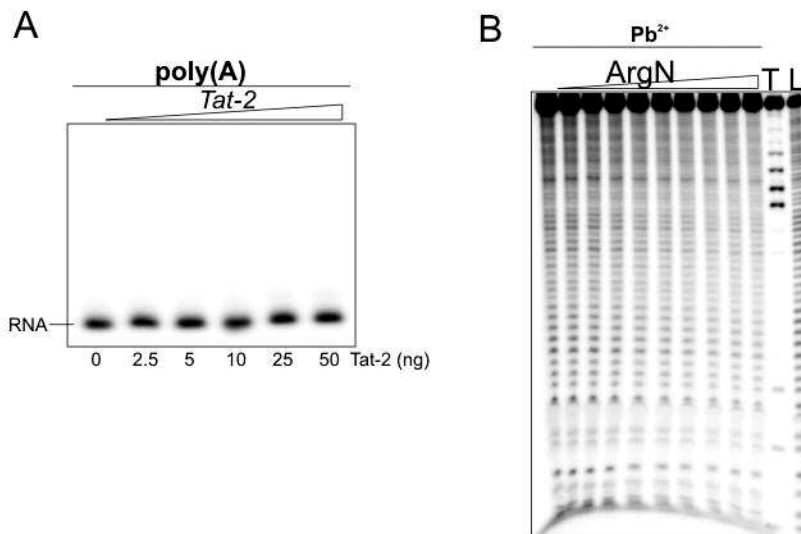


**Figure S10.** The Tat-2 binding (A) and (B) inhibitory effect of argininamide on  $Pb^{2+}$ -induced cleavages for the reference molecule - 60 nt poly(A) RNA. Amounts of the Tat-2 protein (ng per reaction) are indicated below the respective lanes. Lane L represents formamide ladder; lane T, limited hydrolysis with RNase T1.

**Table S1.** Thermodynamic parameters obtained from UV melting experiments for TAR-2 wt and TAR-2 A21 mutant.

	MgCl <sub>2</sub> (mM)	$\Delta H$ (kcal/mol)	$\Delta S$ (cal/Kmol)	$\Delta G$ (kcal/mol) 37°C	T <sub>m</sub> (°C) 1.0e-4M
TAR-2 WILD	0	-86.87±5.937	-260.67±18.204	-6.03±0.299	60.1
	1	-113.67±3.337	-325.14±10.198	-12.83±0.187	76.5
TAR-2 A21 MUTANT	0	-106.72±1.873	-317.71±6.200	-8.18±0.050	62.8
	1	-105.68±2.563	-301.24±7.685	-12.25±0.213	77.7